Cold Regions Science and Technology 151 (2018) 34–46

Contents lists available at ScienceDirect

Cold Regions Science and Technology

journal homepage: www.elsevier.com/locate/coldregions

Considerations on scaling behavior in avalanche flow along cycloidal and parabolic tracks

Peter Gauer

Norwegian Geotechnical Institute, Sognsveien 72, N-0855 Oslo, Norway

ARTICLE INFO

Keywords:
Snow avalanche
Scaling
Similarity
α -β model

ABSTRACT

A simple scaling analysis using a simple mass block model supports observations and measurements on snow avalanches, that the maximum front-velocity of "major" avalanches scales with the total drop height of the track. That is $U_{max} \sim \sqrt{g H_{sc}/2}$ and the average velocity $\overline{U} \approx \frac{2}{\pi} U_{\max}$. The approximation of avalanche tracks as either cycloid or parabola reveal furthermore the connection between the path geometry and the well-known α-β model (Lied and Bakkehøi, 1980). This connection implies a strong dependency of the apparent retardation on the mean steepness of the track. The velocity scaling and the dependency of the retardation on the mean slope angle needs to be reflected in avalanche models.

1. Introduction

Snow avalanches constitute in many alpine areas a serious threat to settlements and infrastructure. Usually, avalanche practitioners use a series of more or less sophisticated dynamical avalanche models to identify areas endangered by avalanches; models like the Voellmy-model (Voellmy, 1955), the PCM-model (Perla et al., 1980), and more recently RAMMS (Christen et al., 2010), SAMOS-AT (Sampl and Granig, 2009) or similar ones. The models are also used to determine forewarn times for, e.g., temporal mitigation measures like traffic lights. However, those models still lack a thorough and documented validation—which is partly caused by the lack of sufficient avalanche data—and therefore, it requires extensive experience from practitioners to assess the model results.

On the other side, Lied and Bakkehøi (1980) proposed a method to estimate the "maximum" avalanche runout distance based only on topographic parameters. To this end, they investigated 423 Norwegian avalanches, which had their maximum extent registered. That is, they looked at "major events" that more or less reached terminus of the path in question. Here and in the following, we use the term "major events" in the sense that these avalanches have return periods of at least several years and can be considered large relative to the path. That means they can be classified as R4 or R5 (cf. Greene et al., 2016, 3.6.5.2 Size - relative to path). In contrast to the often used Canadian avalanche size classification (CASC), which is based on the "destructive force", see McClung and Schaerer (2006) or Greene et al. (2016, 3.6.5.1 Size - destructive force), the relative size classification does not involve an explicit length scale. For this reason, the relative size is more appropriate for the aim of this paper, the study of scaling behavior.

Just a brief remark at this point, whereas the CASC is based on avalanche mass for its categorization, the European Avalanche Warning Services (EAWS) use the deposition volume for its size categorization (c.f. Moner et al., 2013). This can cause a slight difference between both classifications.

Lied and Bakkehøi found that the "Fahrböschungswinkel (Heim, 1932)", the so-called α-angle, can be—in first order—related to the so-called β-angle, which can be regarded as a measure for the mean gradient/slope angle of the avalanche path. In its present form for Norway, the relation for the mean "Fahrböschungswinkel", α_m, for "major" events is given by

$$\alpha_m = 0.96\beta - 1.4^\circ, \tag{1}$$

with a standard deviation $\pm \sigma = 2.3^\circ$. It is noteworthy to say that σ involves both, temporal and spatial variations, due to the variety of considered paths and due to the uncertainty of the return periods of the investigated avalanches. Very similar relations exist for various other countries and regions (McClung and Mears, 1991; Wagner, 2016, and references therein). Common to these statistical relations is that they are independent of any length scale or absolute avalanche size, however they all consider "large" or "major" events (i.e. relative size R4 or R5). These are the sizes that most interest practitioners in hazard mapping.

Recently, Gauer et al. (2010), Gauer (2013, 2014) investigated some scaling relations based on a series avalanche observations from various test-sites, whereby they indicated that the maximum observed front-velocity of major (dry-mixed) avalanches scales as $U_{\max} \sim \sqrt{g H_{sc}}$, where g is the gravitational acceleration and H_{sc} the drop height. Also McClung and Schaerer (2006) suggested a scaling $U_{\max} \propto \sqrt{H_{sc}}$.

E-mail address: peter.gauer@ngi.no.

https://doi.org/10.1016/j.coldregions.2018.02.012
Received 31 July 2017; Received in revised form 18 February 2018; Accepted 27 February 2018
Available online 06 March 2018

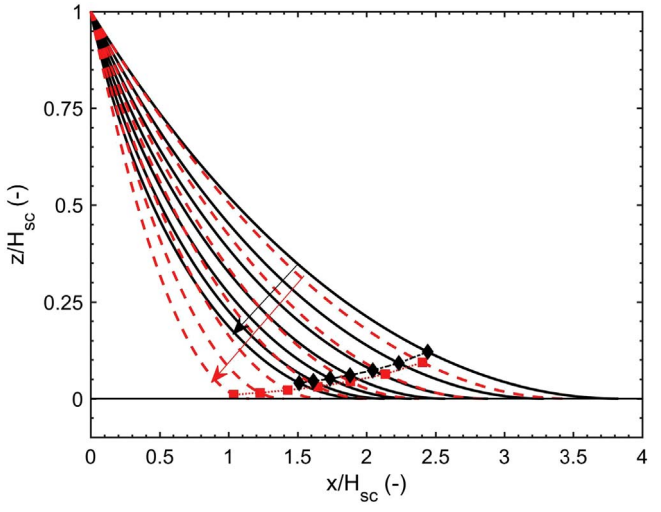

Fig. 1. Comparison between cycloidal (full lines) and parabolic (dashed lines) tracks for initial slope angles, ϕ_0, between 30° and 60° in 5° steps. The tracks are scaled with the maximum drop height, H_{sc}. The markers mark the so-called β-point (see Lied and Bakkehøi, 1980).

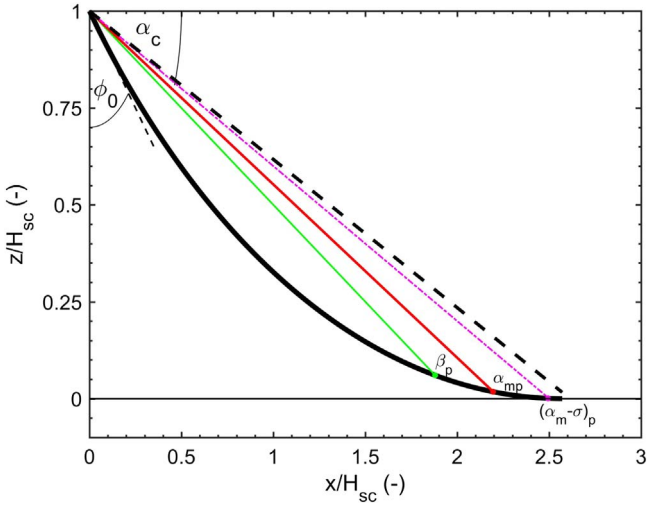

Fig. 2. Cycloidal track scaled by H_{sc} as approximation for an avalanche track. The additional lines connect the top point with the so-called β, α_m, and $\alpha_m - \sigma$ points according to Eq. (1). The black dashed line connects the top with the low point of the cycloid and α_c is the corresponding "Fahrböschungswinkel". In addition ϕ_0 is indicated, which is the initial gradient of the track at its top.

In this paper, we investigate now the scaling behavior of a simple mass block moving along idealized avalanche paths (see Fig. 1). First, we look at the motion along cycloidal paths (Section 2.1) and then along parabolic paths (Section 2.2). Specifically, we look at the relation between runout length and maximum velocity along the track. In this way general trends can be shown.

In order to establish a connection to real avalanche observations at the end, we demonstrate how the α-β model behaves with regard to the runout length on our idealized tracks (Sections 2.1.1 and 2.2.1). For our investigations on the velocity, we focus on two friction laws: 1) a constant retarding acceleration in paragraphs 2.1.2.1 and 2.2.2.1 and 2) a Coulomb friction law in paragraphs 2.1.2.2 and 2.2.2.2. Section 3 tries to provide a compilation of observed trends. To this purpose, either analytical expressions or approximations based on regression analyses of numerical results are provided, or the trends are depict in plots. In particular, Fig. 12 provides an overview on the investigated scaling behavior—if someone wants to look a little ahead. In Section 4, we briefly discuss how the derived scaling behavior relates to real observations and measurements from (dry-mixed) avalanches (i.e. avalanches that are partially fluidized and accompanied by a powder cloud; for more explanation on flow regimes see, e.g., Gauer et al., 2008). To this end, avalanche measurements of runout and velocity are qualitatively compared with results from the scaling analysis.

2. Scaling behavior of a simple mass block model

We base our analysis on a simple mass block model of the form,

$$m\frac{dU}{dt} = m\left(g\sin\phi - a_{ret_e}\right), \tag{2}$$

which is—admittedly—an oversimplification for real avalanche flow. Nonetheless, the model is an admissible first-order approximation and therefore a justifiable proxy for the following scaling analysis. It is similar to the established Voellmy- and PCM-model. Here, U is the velocity of the center of the mass block, m is its mass, g the acceleration due to gravity, and ϕ is the local slope angle. The effective retarding force $m\,a_{ret_e}$ is a measure for the energy dissipation along the track.

2.1. Cycloidal path profile

Many avalanche paths resemble—at least to a first degree—in parts a cycloid. A cycloid is known as the curve of the fastest descent of a mass block under constant gravity. The horizontal and vertical component of the evolute can be described by

$$X_e = R(\Theta - \sin\Theta), \tag{3}$$

$$Z_e = R(1 - \cos\Theta), \tag{4}$$

where Θ corresponds to the angle through which a rolling circle with radius, R, has rotated.

Fig. 2 shows an example of such an "avalanche track" scaled by its maximum drop height H_{sc}. The parameterization for the shown track is given by

$$x(\Theta) = R\left((\Theta - \sin\Theta) - (\Theta_0 - \sin\Theta_0)\right), \tag{5}$$

$$z(\Theta) = R\left(\cos\Theta_0 - \cos\Theta\right), \tag{6}$$

where the relation

$$\Theta = \pi - 2\phi, \tag{7}$$

is used with ϕ in $[\phi_0,0]$. ϕ equals the negative gradient of the track, $\phi = -\arctan(dz/dx)$. The effective drop height is

$$\Delta H_e(\Theta_0, \Theta) = R\left(-\cos\Theta + \cos\Theta_0\right) \tag{8}$$

and the maximum drop height, H_{sc}, of the track is given by

$$\begin{aligned} H_{sc}(\Theta_0) &= \Delta H_e(\Theta_0, \pi), \\ &= R\,(1 + \cos\Theta_0), \\ &= R\,(1-\cos(2\phi_0)), \\ &= 2\,R\sin^2\phi_0. \end{aligned} \tag{9}$$

The distance, S, along the track (i.e. the arc-length) is given by

$$\begin{aligned} S(\Theta_0, \Theta_1) &= \int_{\Theta_0}^{\Theta_1}\sqrt{\left(\frac{dx}{d\Theta}\right)^2 + \left(\frac{dy}{d\Theta}\right)^2}\,d\Theta \\ &= 2R\int_{\Theta_0}^{\Theta_1}\sin(0.5\Theta)\,d\Theta, \end{aligned} \tag{10}$$

or integrated as

$$\begin{aligned} S(\Theta_1, \Theta_0) &= 4\,R\,(\cos(0.5\Theta_0) - \cos(0.5\Theta_1)) \\ &= 4\,R\,(\sin\phi_0 - \sin\phi_1). \end{aligned} \tag{11}$$

2.1.1. α-β model, part I

As reference point for their statistical model, Lied and Bakkehøi (1980) chose—more or less—arbitrarily the β-point, which is defined as

the point, where the gradient to the track,

$$\frac{dz}{dx} = -\frac{\sin\Theta}{1-\cos\Theta} = -\tan\phi, \tag{12}$$

equals $\phi = \phi_\beta = 10^\circ$. With

$$x_\beta = R(2\phi_0 + \sin(2\phi_0) - (\pi/9 + \sin(\pi/9))), \tag{13}$$

$$z_\beta = R(-\cos(2\phi_0) + \cos(\pi/9)), \tag{14}$$

tanβ can be expressed by

$$\tan\beta = \frac{z_\beta}{x_\beta} = \frac{-\cos(2\phi_0) + \cos(\pi/9)}{2\phi_0 + \sin(2\phi_0) - (\pi/9 + \sin(\pi/9))}, \tag{15}$$

or using $\gamma_{1\beta} = (\pi/18 - \phi_0)$ and $\gamma_{2\beta} = (\pi/18 + \phi_0)$

$$\tan\beta = \frac{\sin\gamma_{2\beta}}{\gamma_{1\beta}/\sin\gamma_{1\beta} + \cos\gamma_{2\beta}}. \tag{16}$$

Due to the fortunate choice of the β-point, the β-angle is almost linear related to relevant ϕ_0 angles,

$$\beta \approx 0.42\phi_0 + 6.\,8^\circ, \tag{17}$$

with ($R = 0.98$; $\sigma_f = 0.09^\circ$). As mentioned, ϕ_0 is the gradient of the track in the "release area", which is typically in the range of [30°,55°]. Both, the β-angle and ϕ_0, can be regarded as a measure for the steepness of the track.

Similar to Eq. (15), the runout angle α ("Fahrböschungswinkel") is given by

$$\tan\alpha = \frac{z_\alpha}{x_\alpha} = \frac{-\cos(2\phi_0) + \cos(2\phi_\alpha)}{2\phi_0 + \sin(2\phi_0) - (2\phi_\alpha + \sin(2\phi_\alpha))}, \tag{18}$$

or using $\gamma_{1\alpha} = (\phi_\alpha - \phi_0)$ and $\gamma_{2\alpha} = (\phi_\alpha + \phi_0)$

$$\tan\alpha = \frac{\sin\gamma_{2\alpha}}{\gamma_{1\alpha}/\sin\gamma_{1\alpha} + \cos\gamma_{2\alpha}}, \tag{19}$$

where $\phi_\alpha = -\arctan(dz_\alpha/dx_\alpha)$ (i.e. ϕ_α is the slope angle of the track at the point (x_α, z_α)). Therefore, ϕ_0 and ϕ_α can be used to parameterize the runout on our idealized track. In the case the avalanche stops in the valley bottom, that is at the low point of the cycloid where $\phi_\alpha = 0$, one obtains for the "Fahrböschungswinkel" α_c

$$\tan\alpha_c = \frac{1 - \cos(2\phi_0)}{2\,\phi_0 + \sin(2\,\phi_0)} = \sin\left(0.5\,\phi_0\right). \tag{20}$$

Otherwise,

$$\tan\alpha \approx -0.02 + 1.07\sin(0.5\phi_0) + 1.24\sin(0.5\phi_\alpha) \tag{21}$$

gives a first approximation. For ϕ_0 in the range of 25° to 60°, which covers the slope angle of typical release areas,

$$\alpha_c \approx 0.42\phi_0 + 2.\,2^\circ. \tag{22}$$

Combining Eqs. (15) and (18) one can obtain a relationship for α_c depending on the β angle,

$$\alpha_c \approx 0.97\beta - 4.\,6^\circ, \tag{23}$$

which is quite similar to the one obtained by Lied and Bakkehøi (1980) for $\alpha_m - \sigma$. Fig. 3 shows the comparison between the Norwegian α-β relation (1) and the relation for α_c in Eq. (23).

2.1.2. Mass block model—energy considerations, part I

Until now we looked at some geometrical relations that follow directly from the idea behind the statistical α-β model. In this section now, we discus some dynamic aspects that result. To this end, we look at a simple mass block moving down the track. The energy balance of the mass block is given by

$$\frac{1}{2}mv^2 = m\,(g\Delta z - e_{Dis}), \tag{24}$$

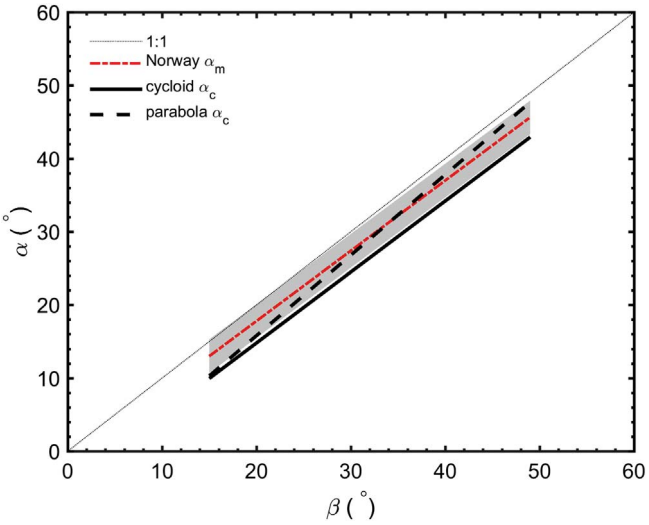

Fig. 3. Comparison of α-β relations according to Eq. (1) and relations (23) and (77). The red dash-dotted line shows the fit by Lied and Bakkehøi (1980) and the gray-shaded area marks the corresponding ± σ-range. (For interpretation of the references to color in this figure legend, the reader is referred to the web version of this article.)

where $e_{Dis} = \int_0^S a_{ret}(s)\,ds$ marks the energy dissipated per unit mass along the track with an arc-length S. Δz is the vertical drop. Here, we also assume that the initial velocity is zero. The mean retarding acceleration

$$\bar{a}_{ret} = \frac{1}{S_1}\int_0^{S_1} a_{ret}(s)\,ds, \tag{25}$$

which is based on the relation for the energy balance from start to stop

$$0 = \int_{x_0}^{x_1}\left(g\frac{dz}{dx} - \frac{d(a_{ret}\,s)}{dx}\right)dx, \tag{26}$$

where x_0 is the horizontal start and x_1 the stopping position. This implies, the total potential energy is dissipated along the arc-length S_1. For a cycloidal track, one obtains

$$\begin{aligned}\frac{\bar{a}_{ret}(\Theta_1, \Theta_0)}{g} &= \frac{1}{4}\frac{\cos(\Theta_0) - \cos(\Theta_1)}{\cos(0.5\Theta_0) - \cos(0.5\Theta_1)} \\ &= 0.5(\sin\phi_0 + \sin\phi_1),\end{aligned} \tag{27}$$

where ϕ_1 is the negative gradient of track at the stopping position. In the special case $\Theta_1 = \pi$ (i.e. $\phi_1 = 0$), this is

$$\begin{aligned}\frac{\bar{a}_{ret}}{g} &= 0.5\sin\phi_0 \\ &\approx 0.94\sin\beta - 0.07.\end{aligned} \tag{28}$$

This relation is similar and shows the same tendency to the one proposed by Gauer et al. (2010)

$$\frac{a_{ret\,m}}{g} \approx 0.82\sin\beta + 0.05, \tag{29}$$

with $\pm\,\sigma/g = 0.04$, which they derived from avalanche observations and measurements. Both relations are shown in Fig. 4.

2.1.2.1. Mass block with constant retarding acceleration $a_{ret} = const.$.

Let us first focus on a mass block moving with a constant retarding acceleration.

Maximum velocity. To derive an expression for maximum velocity, we start from the relation

$$v = \sqrt{2g\,(\Delta z - a_{rg}s)}, \tag{30}$$

which is based on the energy balance (24) and where we use the abbreviation $a_{rg} = a_{ret}/g$. For the cycloidal track, Eq. (30) equals

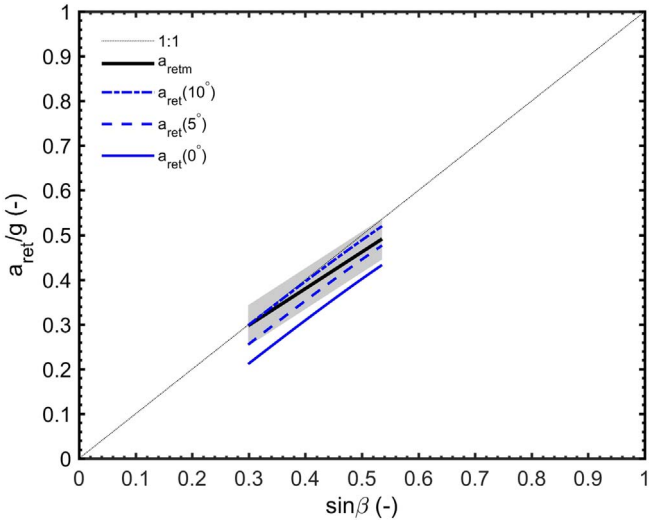

Fig. 4. Comparison of a_{ret} according to relation (28) with ϕ_1 as parameter and relation (29). The gray-shaded area marks the ± σ-range of Eq. (29).

$$\frac{ds}{dt} = \sqrt{2gR\,((\cos\Theta_0 - \cos\Theta) - 4\,a_{rg}(\cos(0.5\Theta_0) - \cos(0.5\Theta)))}, \tag{31}$$

with $v = \frac{ds}{dt}$. The maximum velocity along the track can be found by using the prerequisite

$$\frac{d^2s}{dt^2} = \frac{2gR(\sin\Theta - 2a_{rg}\sin(0.5\Theta))\,d\Theta/dt}{\sqrt{2gR\,((\cos\Theta_0 - \cos\Theta) - 4a_{rg}(\cos(0.5\Theta_0) - \cos(0.5\Theta)))}} = 0, \tag{32}$$

from which the condition follows that

$$\begin{aligned} a_{rg} &= \cos(0.5\Theta) \\ &= \frac{0.5\sin\Theta}{\sin(0.5\Theta)} \\ &= 0.5(\cos(0.5\Theta_0) + \cos(0.5\Theta_1)). \end{aligned} \tag{33}$$

Using now Eq. (33) in Eq. (31) one obtains a relation for the maximum velocity along the track

$$U_{\max} = \sqrt{g\,R}\,(\cos(0.\,5\Theta_0) - \cos(0.\,5\Theta_1)), \tag{34}$$

or

$$U_{\max} = \sqrt{g\,\Delta H_e}\,\frac{(\cos(0.5\Theta_0) - \cos(0.5\Theta_1))}{\sqrt{(\cos(\Theta_0) - \cos(\Theta_1))}}. \tag{35}$$

Relating Eq. (35) to the maximum drop height H_{sc} (cf. Eq. (9)), gives

$$\begin{aligned} U_{\max} &= \sqrt{\frac{g\,H_{sc}}{2}}\left(1 - \frac{\cos(0.5\Theta_1)}{\cos(0.5\Theta_0)}\right) \\ &= \sqrt{\frac{g\,H_{sc}}{2}}\left(1 - \frac{\sin\phi_1}{\sin\phi_0}\right). \end{aligned} \tag{36}$$

For $\Theta_1 = \pi$, it follows

$$\frac{U_{\max}}{\sqrt{g\,H_{sc}}} = \frac{1}{\sqrt{2}}. \tag{37}$$

That means, for an avalanche on cycloidal track, which reaches the valley bottom and has a constant retarding acceleration, the scaled maximum velocity is independent of the actual steepness of the track. Relation (36) is included in Fig. 12.

Travel time. Using Eq. (30), the travel time of a mass block down the track is given by

$$\int_0^{t_a} dt = \int_0^{S_1} \frac{ds}{\sqrt{2\,(g\,\Delta z - a_{ret}(s)\,s)}}. \tag{38}$$

For a cycloid path the travel time is

$$t_a = \sqrt{\frac{2R}{g}}\int_{\Theta_0}^{\Theta_1} \frac{\sin(0.5\Theta)\,d\Theta}{\sqrt{(\cos\Theta_0 - \cos\Theta) - 4\,a_{rg}(\Theta_0, \Theta)(\cos(0.5\Theta_0) - \cos(0.5\Theta))}}. \tag{39}$$

If one assumes that $a_{rg}(\Theta_0,\Theta)$ is constant along the track, in which case $a_{rg} = 0.5\ (\sin\phi_0 + \sin\phi_1) = 0.5\ (\cos(0.5\Theta_0) + \cos(0.5\Theta_1))$, one obtains for an avalanche descending along of a cycloidal track

$$\begin{aligned} t_a &= \sqrt{2}\,\pi\,\sqrt{\frac{2R}{g}} \\ &= \sqrt{2}\,\pi\sqrt{\frac{2\Delta H_e}{g(\cos\Theta_0 - \cos\Theta_1)}} \end{aligned} \tag{40}$$

and related to the maximum drop height, H_{sc},

$$t_a = \frac{\sqrt{2}\,\pi}{\sin\phi_0}\sqrt{\frac{H_{sc}}{g}}. \tag{41}$$

This means the travel time is independent ϕ_1; that is t_a time is independent of the actual runout distance. This phenomenon is known as isochronous. However, the travel time depends on the steepness of the track. On a shallower track avalanches take longer. Relation (41) is also included in Fig. 12.

Mean velocity. Finally, the mean velocity can be found by

$$\overline{U} = \frac{S(\Theta_0, \Theta_1)}{t_a}, \tag{42}$$

which gives the relations

$$\begin{aligned} \overline{U} &= \frac{2\sqrt{g\,R}}{\pi}(\cos(0.5\Theta_0) - \cos(0.5\Theta_1)), \\ &= \frac{2\sqrt{g\,\Delta H_e}}{\pi}\frac{(\cos(0.5\Theta_0) - \cos(0.5\Theta_1))}{\sqrt{\cos(\Theta_0) - \cos(\Theta_1)}}, \\ &= \frac{2}{\pi}\sqrt{\frac{g\,H_{sc}}{2}}\left(1 - \frac{\sin\phi_1}{\sin\phi_0}\right). \end{aligned} \tag{43}$$

For $\Theta_1 = \pi$, one obtains

$$\overline{U} = \frac{2}{\pi}\sqrt{\frac{g\,H_{sc}}{2}} \tag{44}$$

Comparing Eq. (36) with Eq. (43) one recognizes, that in all cases, the mean velocity is

$$\overline{U} = \frac{2}{\pi}\,U_{\max}. \tag{45}$$

As an illustration, Fig. 5 shows an example of the velocity distribution of a mass block with constant retarding acceleration moving along a cycloidal track. For comparison, the apparent friction factor μ_a ($= a_{ret}/g\cos\phi$) is shown, that is the variable friction factor that a Coulomb model needs, to behave like a model with constant retarding acceleration.

2.1.2.2. Mass block with Coulomb friction $a_{ret} = \mu\,g\,\cos\phi$. In this section, we consider a mass block sliding with Coulomb friction. This is probably one of the first mathematical descriptions for the motion of an avalanche, proposed by Prof. M. Rosenmund (cited in Coaz, 1910).

Friction parameter μ. Simple energy considerations for a mass block require that potential energy between start and stopping position is dissipated along the track, that is

$$g\,\Delta H_e = 2\,g\,\mu\,R\int_{\Theta_0}^{\Theta_1}\sin^2(0.5\Theta)\,d\,\Theta. \tag{46}$$

Here, we use again relation (10) and $\cos\phi = \sin(0.5\ \Theta)$. Further, using Eq. (8), one obtains the relation

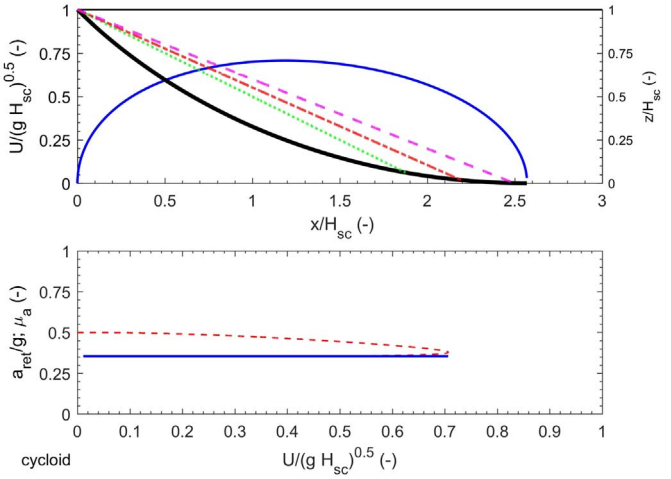

Fig. 5. Upper panel, velocity of a mass block (blue line) moving with a constant retarding acceleration along a cycloidal track (black line, $\phi_0 = 45°$) and reaching the "valley bottom". The green-dotted line marks the β-point, and the dash-dotted red line and the dashed magenta line depict the α_m- and α_m–σ-points according to Eq. (1). The lower panel shows the retarding acceleration, a_{ret} (blue line), and the corresponding apparent friction factor, $\mu_a = a_{ret}/g\cos\phi$ (red dashed line). (For interpretation of the references to color in this figure legend, the reader is referred to the web version of this article.)

$$\mu = \frac{\cos\Theta_0 - \cos\Theta_1}{(\Theta_1 - \sin\Theta_1) - (\Theta_0 - \sin\Theta_0)}, \tag{47}$$

which depends on the start and stopping position. Using $\gamma_1 = (\Theta_1 - \Theta_0)/2$ and $\gamma_2 = (\Theta_1 + \Theta_0)/2$

$$\mu = \frac{\sin\gamma_2}{\gamma_1/\sin\gamma_1 - \cos\gamma_2}, \tag{48}$$

and in the case $\Theta_1 = \pi$, this is

$$\mu = \sin(0.5\phi_0) \tag{49}$$

For small ϕ_1,

$$\mu \approx 0.02 + 0.9\sin(0.5\phi_0) + 1.05\sin(0.5\phi_1). \tag{50}$$

Based on avalanche observations, Gauer et al. (2010) suggested that the friction coefficient μ_0 for a Coulomb model should vary, like

$$\mu_0 \approx 0.82\tan\beta + \frac{0.52}{\cos\beta}. \tag{51}$$

Fig. 6 shows a comparison between relations (48) and (51), where β is given by Eq. (17).

Maximum velocity. Following the same approach as above, one can derive the relation for the maximum velocity, starting with

$$\frac{ds}{dt} = \sqrt{2gR\,((\cos\Theta_0 - \cos\Theta) - \mu((\Theta - \sin\Theta) - (\Theta_0 - \sin\Theta_0)))}, \tag{52}$$

where we use $\int_{\Theta_0}^{\Theta}\sin^2(0.5\Theta)\,d\Theta$. The prerequisite

$$\frac{d^2s}{dt^2} = \sqrt{\frac{g\,R}{2}}\,\frac{\sin\Theta - \mu(1 - \cos\Theta)}{\sqrt{((\cos\Theta_0 - \cos\Theta) - \mu((\Theta - \sin\Theta) - (\Theta_0 - \sin\Theta_0)))}} = 0 \tag{53}$$

provides a condition for the location of the maximum velocity to occur:

$$\mu = \cot(0.5\Theta) = \tan\phi. \tag{54}$$

Using Eq. (54) in Eq. (52), one can obtain an approximation for the maximum velocity along the track

$$U_{\max} \approx \sqrt{2\,g\,R}\,(0.0315 + 0.635\phi_0 - 0.655\phi_1), \tag{55}$$

or

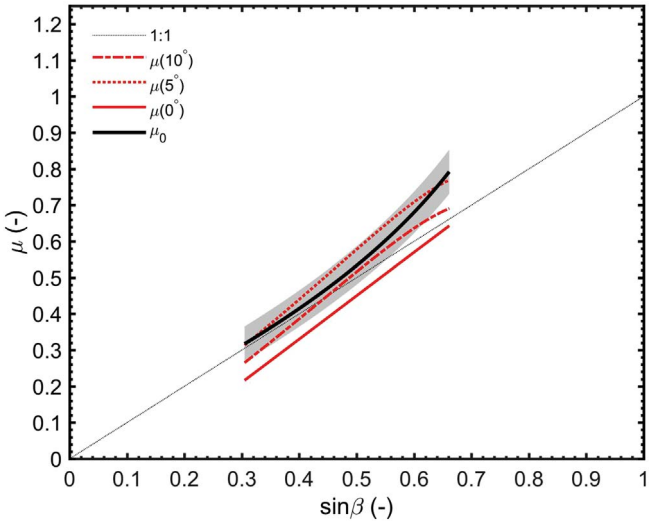

Fig. 6. Comparison of μ according to relation (48) with $\phi_1 = [0°,5°,10°]$ and relation (51). The gray-shaded area marks the $\pm\,\sigma$-range of Eq. (51).

$$U_{\max} \approx \sqrt{2\,g\,\Delta H_e}\,\frac{(0.0315 + 0.635\phi_0 - 0.655\phi_1)}{\sqrt{\sin(2\phi_0) - \sin(2\phi_1)}}. \tag{56}$$

Related to the maximum drop height H_{sc} (see Eq. (9)), it is

$$U_{\max} \approx \sqrt{\frac{gH_{sc}}{2}}\left(\frac{0.044 + 0.9\phi_0 - 0.92\phi_1}{\sin\phi_0}\right). \tag{57}$$

The approximations are based on regression analyses of numerical results.

Travel time. Further, one obtains the relation for the travel time:

$$t_a = \sqrt{\frac{2R}{g}}\int_{\Theta_0}^{\Theta_1}\frac{\sin(0.5\Theta)\,d\Theta}{\sqrt{(\cos\Theta_0 - \cos\Theta) - 4\,\mu(\Theta - \sin\Theta - (\Theta_0 - \sin\Theta_0))}}. \tag{58}$$

This might be approximated by

$$t_a \approx \sqrt{2}\,\pi\,\sqrt{\frac{2R}{g}}\,(0.77 + 0.22\cos\phi_0)(1 - 0.28\,\sin\phi_0\tan\phi_1), \tag{59}$$

or, when related to the maximum drop height, by

$$t_a \approx \frac{\sqrt{2}\,\pi}{\sin\phi_0}\,\sqrt{\frac{H_{sc}}{g}}\,(0.77 + 0.22\cos\phi_0)(1 - 0.28\,\sin\phi_0\tan\phi_1). \tag{60}$$

In this case, the travel time is depending on the steepness and the actual runout distance.

Mean velocity. Finally, the mean velocity,

$$\overline{U} = \frac{S(\phi_0, \phi_1)}{t_a}, \tag{61}$$

is again around

$$\overline{U} \approx \frac{2}{\pi}U_{\max}. \tag{62}$$

2.2. Parabola (polynomial 2 degree)

In one of the original papers, Bakkehøi et al. (1983) used a second degree function of the type

$$z = a\,x^2 + b\,x + c \tag{63}$$

to fit the avalanche tracks for their analysis (see Fig. 7). A closer look reveals the connections between the parameters of the parabola and the α-β model. The horizontal distance x_m to the low point is

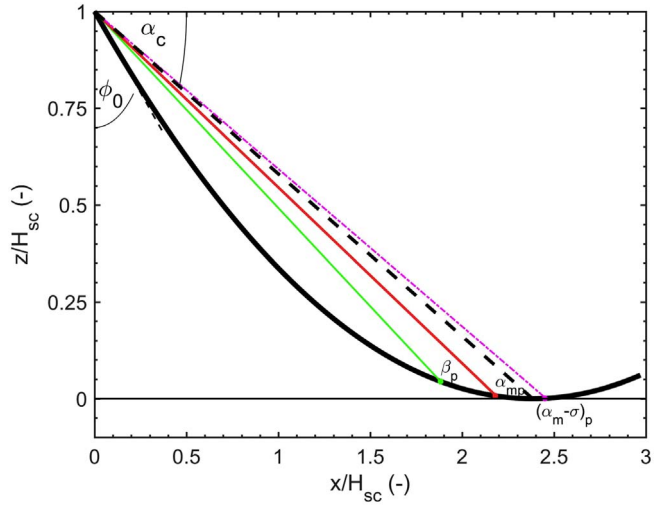

Fig. 7. Parabolic track scaled by H_{sc} as approximation for an avalanche track. The additional lines connect the top point with the so-called β, α_m, and $\alpha_m - \sigma$ points according to Eq. (1). The black dashed line connects the top with the low point of the parabola and α_c is the corresponding "Fahrböschungswinkel". In addition ϕ_0 is shown, which is the gradient of the track at its top.

$$x_m = -\frac{b}{2a}, \tag{64}$$

and the elevation of the low point

$$z_m = \frac{b^2}{4a} + c. \tag{65}$$

With $H_{sc} = z_0 - z_m$, where z_0 is the elevation of the "release area" and

$$H_{sc} = \frac{b^2}{4a}, \tag{66}$$

the offset, c, is

$$c = z_m + \frac{b^2}{4a}. \tag{67}$$

Finally, the steepness of the "release area" (i.e. the negative gradient) is

$$\tan\phi_0 = -\sqrt{2\,z^{''}\,H_{sc}} = -b, \tag{68}$$

where $z^{''} = 2a$, and from Eq. (66) it follows

$$a = \frac{\tan^2\phi_0}{4H_{sc}}. \tag{69}$$

Combining Eqs. (64)–(69), Eq. (63) can be rewritten as

$$z = \frac{\tan^2\phi_0}{4\,H_{sc}}\,x^2 - \tan\phi_0\,x + H_{sc} + z_m, \tag{70}$$

and

$$\Delta z = -\frac{\tan^2\phi_0}{4\,H_{sc}}\,x^2 + \tan\phi_0\,x. \tag{71}$$

2.2.1. α-β model, part II

For a parabola, the so-called β-point is found similar to Eq. (15) by

$$\tan\beta = \frac{\Delta z_{10}}{x_{10}} = \frac{\tan(\pi/18) + \tan\phi_0}{2}. \tag{72}$$

As in the case of the cycloid track approximation, the β-angle is also in the case of a parabola almost linear related to ϕ_0 in the relevant range (i.e. ϕ_0 = [30,55]),

$$\beta \approx 0.72\phi_0 - 1.\,4°, \tag{73}$$

with ($R = 0.98$; $\sigma_f = 0.37°$). In the case that the avalanche stops in the "valley bottom", one obtains for the runout angle (i.e. "Fahrböschungswinkel")

$$\tan\alpha_c = \frac{H_{sc}}{x_m} = -\frac{b}{2} = \frac{\tan\phi_0}{2}. \tag{74}$$

Otherwise α is given by

$$\begin{aligned}\tan\alpha &= \frac{\Delta H_e}{x_\alpha}\\ &= -\frac{\tan^2\phi_0}{4H_{sc}}x_\alpha + \tan\phi_0\,,\\ &= \frac{\tan\phi_0 + \tan\phi_\alpha}{2},\end{aligned} \tag{75}$$

where we use the relation $\tan\phi_\alpha = -dz_\alpha/dx_\alpha$. Here again, we use ϕ_α instead of ϕ_1 to emphasize that there is a unique relation between the slope angle for a parabola and α. Combining Eqs. (72) and (75) yields

$$\tan\alpha = \tan\beta + \frac{\tan\phi_\alpha - \tan(\pi/18)}{2}. \tag{76}$$

For the range of interest for $\tan\phi_0$, this ensures a nearly linear relation

$$\alpha_c \approx 1.1\beta - 6.\,4°, \tag{77}$$

which is included in Fig. 3.

2.2.2. Mass block model—energy considerations part II

Following the same line of argumentation as in Section 2.1.2, one obtains the relation for the mean retarding acceleration

$$\frac{\bar{a}_{ret}(\phi_1, \phi_0)}{g} = \frac{\Delta H_e}{S}, \tag{78}$$

where ϕ_0 and ϕ_1 are the slope angles (i.e. the negative gradient $-\arctan(dz/dx)$) of the start and stopping position, respectively. The arc-length, S, can be calculated using

$$S = \int_0^{x_1} \sqrt{1 + (2ax + b)^2}\;dx. \tag{79}$$

This gives

$$S(x_1) = \frac{1}{4a}(X\sqrt{1 + X^2} + \operatorname{arcsinh}(X)) - \frac{1}{4a}(b\sqrt{1 + b^2} + \operatorname{arcsinh}(b)), \tag{80}$$

where the tangents of the local slope angle is $X = (2ax_1 + b)$. From this, one obtains

$$\begin{aligned}\frac{\bar{a}_{ret}(\phi_1, \phi_0)}{g} = \frac{1 - \frac{\tan^2\phi_1}{\tan^2\phi_0}}{(\tan(-\phi_1)\sqrt{1 + \tan^2(-\phi_1)} + \operatorname{arcsinh}(\tan(-\phi_1)))}\\ - (\tan(-\phi_0)\sqrt{1 + \tan^2(-\phi_0)} + \operatorname{arcsinh}(\tan(-\phi_0)))\end{aligned} \tag{81}$$

which might be approximated by

$$\frac{\bar{a}_{ret}(\phi_1, \phi_0)}{g} \approx 1.1 - 0.95\cos\phi_0 + 0.37\tan\phi_1 \tag{82}$$

and for $\phi_1 = 0$ as

$$\frac{\bar{a}_{ret}}{g} \approx 1.05\sin\beta - 0.095. \tag{83}$$

Fig. 8 shows the comparison between relation (82) and Eq. (29).

2.2.2.1. Mass block with constant retarding acceleration a_{ret} = const.. Let us again first focus on a mass block moving with a constant retarding acceleration.

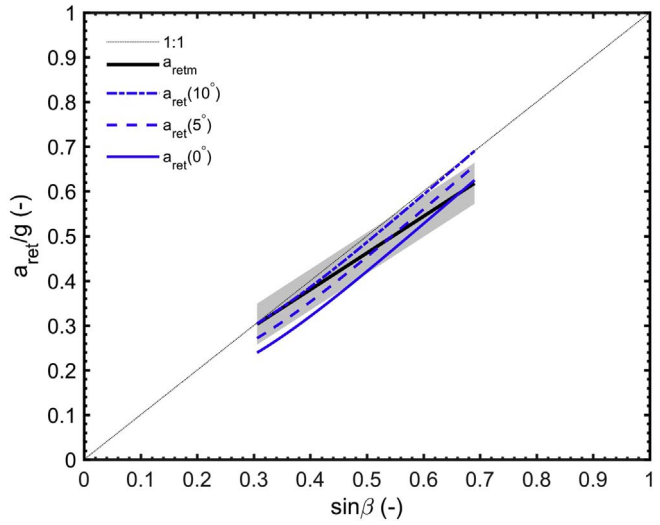

Fig. 8. Comparison of a_{ret} according to relation (82) with ϕ_1 as parameter and Eq. (29). The gray-shaded area marks the ± σ-range of Eq. (29).

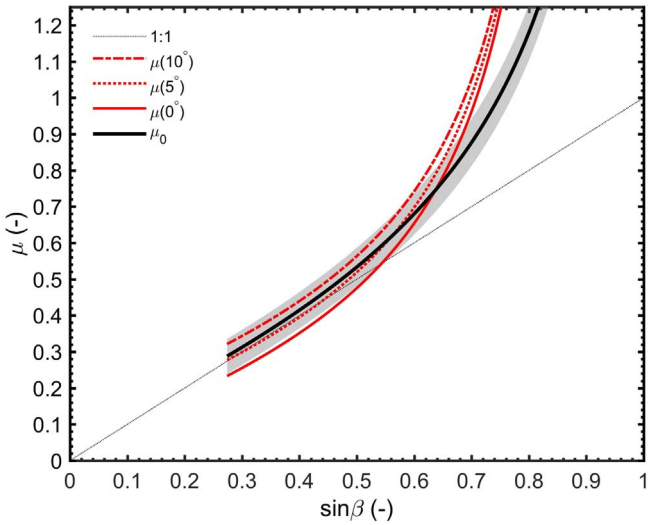

Fig. 9. Comparison of μ according to relation (92) with $\phi_1 = [0°,5°,10°]$ and relation (51). The gray-shaded area marks the ± σ-range of Eq. (51).

Maximum velocity. Starting from energy balance (24), the velocity along the track is

$$\frac{ds}{dt} = \sqrt{2g\ (\Delta z - a_{rg} s)}, \tag{84}$$

where $a_{rg} = \bar{a}_{ret}/g$. Following the same line of argumentation as in Section 2.1.2.1 (i.e. exploring the condition $d^2s/dt^2 = 0$), one obtains the condition where along the track the maximum velocity occurs:

$$X = \frac{a_{rg}}{\sqrt{1 - a_{rg}^2}}. \tag{85}$$

Here, we use the abbreviation for the local gradient $X = 2ax + b$. With this and Eqs. (84), (80), and (71), the maximum velocity can be approximated by

$$U_{\max} \approx \sqrt{\frac{g\ H_{sc}}{2}} \left(1.05 + 0.16 \tan\phi_1 - 0.15 \tan\phi_0 - 1.1 \frac{\tan\phi_1}{\tan\phi_0}\right). \tag{86}$$

Again, the approximation is based on a regression analysis of numerical results.

Travel time. The travel time is found by using

$$\int_0^{t_a} dt = \int_0^{s_1} \frac{ds}{\sqrt{2\ (g\ \Delta z - a_{ret}(s)\ s)}}, \tag{87}$$

which provides the estimate

$$t_a \approx \pi \sqrt{\frac{2\ H_{sc}}{g}} (0.52 + 0.81 \cot\phi_0 + 0.43 \tan\phi_1). \tag{88}$$

The travel time is depending on the steepness as well as on the actual runout distance.

Mean velocity. The mean velocity is given by

$$\overline{U} = \frac{S(\phi_0, \phi_1)}{t_a} \tag{89}$$

and is again

$$\overline{U} \approx \frac{2}{\pi} U_{\max}. \tag{90}$$

2.2.2.2. Mass block with Coulomb friction $a_{ret} = \mu\ g\ cos\phi$. In this section, we consider a mass block sliding with constant Coulomb friction. The respective friction parameter is found again by energy considerations similar to Eq. (46), that is

$$g\Delta H_e - \int_{x_0}^{x_1} g\ \mu\ dx = 0, \tag{91}$$

where $dx = ds/\cos\phi$. Using $\tan\phi_1 = -dz_1/dx_1$, one obtains

$$\mu = \frac{\tan\phi_0 + \tan\phi_1}{2}. \tag{92}$$

Fig. 9 shows a comparison between relations (92) and (51), where β is given by Eq. (73).

Maximum velocity. The velocity along the track is

$$\frac{ds}{dt} = \sqrt{2\ g \left(\frac{-\tan^2\phi_0}{4H_{sc}} x^2 + \tan\phi_0\ x - \mu\ x\right)}. \tag{93}$$

The maximum velocity is found using once again the prerequisite $d^2s/dt^2 = 0$, which provides the condition

$$\mu = \tan\phi = \frac{\tan\phi_0 + \tan\phi_1}{2}. \tag{94}$$

Using Eq. (94) in Eq. (93), gives the relation for the maximum velocity

$$U_{\max} = \sqrt{\frac{g\ H_{sc}}{2}} \left(1 - \frac{\tan\phi_1}{\tan\phi_0}\right). \tag{95}$$

Travel time. Using Eq. (38), the travel time of a mass block with Coulomb friction along a parabolic track is given by

$$\int_0^{t_a} dt = \frac{1}{\sqrt{2\ g}} \int_0^{x_1} \frac{\sqrt{1 + (2ax + b)^2}\ dx}{\sqrt{(-a\ x^2 - bx - \mu\ x)}}, \tag{96}$$

which is around

$$t_a \approx \frac{\pi}{\sin\phi_0} \sqrt{\frac{2H_{sc}}{g}} (0.41 + 0.58 \cos\phi_0), \tag{97}$$

where we disregard a slight dependency on ϕ_1.

Mean velocity. The mean velocity is found by

$$\overline{U} = \frac{S(\phi_0, \phi_1)}{t_a} \tag{98}$$

and yields

$$\overline{U} \approx \frac{2}{\pi} U_{\max}. \tag{99}$$

Fig. 10 plots an example of the velocity distribution of a mass block with constant Coulomb friction moving along a parabolic track. For

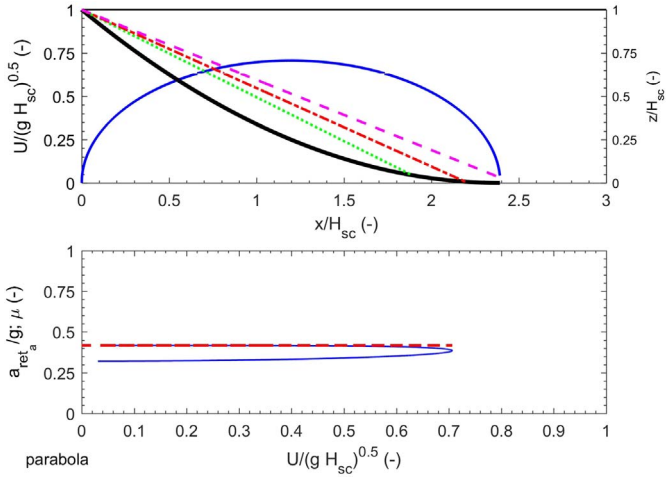

Fig. 10. Upper panel, velocity (blue line) of a mass block moving with a constant Coulomb friction along a cycloidal track (black line, $\phi_0 = 45°$) and reaching the "valley bottom". The green-dotted line marks the β-point, and the dash-dotted red line and the dashed magenta line depict the α_m- and α_m–σ-points according to (1). The lower panel shows the Coulomb friction factor, μ (red dashed line), and the corresponding apparent retarding acceleration, $a_{ret_a} = \mu g \cos\phi$ (blue line). (For interpretation of the references to color in this figure legend, the reader is referred to the web version of this article.)

comparison, the apparent retarding acceleration $a_{ret_a}(=\mu g \cos\phi)$ is shown, that is the variable retarding acceleration that a mass block needs, to behave like a pure Coulomb model.

3. Compilation of observed trends

In this section, we provide a summary of the main results from our scaling analysis. The following Tables 1 to 3 present either analytical expressions or approximations based on regression analyses of numerical results. Table 1 gives a brief overview of typical geometrical relations or their approximations for a cycloid and a parabola.

Table 2 summarizes the relation between the geometry of the track and a representative α-angle, for which we choose the gradient between high and low point of the track (α_c).

To repeat some of the underlying thoughts of our scaling analysis in Section 2. Basic energy considerations provide a relation between the mean retarding force and the stopping position of an avalanche. For our simple mass block model this relation is

$$\frac{\overline{a}_{ret}}{g} = \frac{\Delta H_e}{S_1}. \tag{100}$$

This means, a mass block with a constant retarding acceleration equal to $\overline{a}_{ret}$ will stop at a distance S_1. For a mass block with constant Coulomb friction, Eq. (100) provides also a condition for the required friction factor

Table 2
α-β approximation with ϕ_0 and β-angle as reference for a cycloidal and parabolic track, respectively. Here, α_c is the "Fahrböschungswinkel" to the low point.

Reference	Cycloid	Parabola
ϕ_0	$\tan\alpha_c = \sin(0.5\phi_0)$	$\tan\alpha_c = 0.5\tan\phi_0$
ϕ_0	$\alpha_c \approx 0.42\phi_0 + 2.2°$	$\alpha_c \approx 0.78\phi_0 - 7.8°$
β-angle	$\alpha_c \approx 0.97\beta - 4.6°$	$\alpha_c \approx 1.1\beta - 6.4°$

$$\mu = \frac{\Delta H_e}{x_1} = \frac{\overline{a}_{ret}}{g}\frac{S_1}{x_1}. \tag{101}$$

These relations are independent of the actual form of the track and are not restricted to our idealizations.

Fig. 11 shows contour plots of the required $\overline{a}_{ret}$ and μ values depending on given start and stopping positions, which are parameterized by ϕ_0 and ϕ_1, for our idealized avalanche tracks. The lower panel in the figure shows the same data, however, related to the β-angle, which is by practitioners more commonly used. As mentioned above, the β-angle can be regarded as a measure for the mean steepness of the track. Cycloids with large initial gradients (i.e. large ϕ_0) are on average less steep than their parabolic counterparts. This is seen Fig. 1 and this is the reason why in Fig. 11, ϕ_0 is mirrored in a much smaller range of β-angles in the case of cycloids than for parabolas.

The dependency of $\overline{a}_{ret}$ or μ on the steepness of the track supports suggestions that those parameters reflect rather dynamical than pure material behavior. Considering the idea behind the α-β model, all runouts with ϕ_1 in the gray areas or to the right reflect large or "major" events (size R4 or R5), whereby the gray areas themselves mark the most probable range for these size classes.

Avalanche models like the Voellmy-model (Voellmy, 1955) and the PCM-model (Perla et al., 1980) introduce a notable velocity dependency of the retardation. Energy consideration can provide some constraints for the parameter choice of these models and yield an expression for the mean retarding acceleration (see also discussion in Gauer, 2014),

$$\frac{\overline{a}_{ret}}{g} = \mu\frac{x_1}{S_1} + c a_2 H_{sc}. \tag{102}$$

In the case of a PCM-type model, $a_2 \equiv D/M$ and for a Voellmy-type model $a_2 \equiv g/\xi\, h$. D/M is a lumped friction parameter whereas in the Voellmy-type model the flow height, h, occurs explicitly and ξ is the so-called turbulent friction parameter. Here, we will also use the observation that $\overline{U^2} \gtrsim \overline{U}^2 \sim 2gH_{sc}/\pi^2$ from which follows that the factor $c \gtrsim 0.2$ (or using the approximation $\sqrt{\overline{U^2}} \approx 0.81 U_{\max}$ for which $c \approx 0.33$ yields).

First of all, Eq. (102) implies that the choice of the parameter for the Coulomb friction part and for the velocity dependent part—in the Voellmy- as well as in the PCM-type model—is not independent. Secondly, looking at Fig. 11, typical values of $\overline{a}_{ret}/g$ range between 0.25

Table 1
Typical geometrical relations for cycloidal and parabolic tracks or their (rough) approximations.

Parameter	Cycloid	Parabola
β	$\approx 0.42\phi_0 + 6.8°$	$\approx 0.72\phi_0 - 1.4°$
$\Delta H_e/H_{sc}$	$= 1 - \frac{\sin^2\phi_1}{\sin^2\phi_0}$	$= 1 - \frac{\tan^2\phi_1}{\tan^2\phi_0}$
$S_1/\Delta H_e$	$= \frac{2}{\sin\phi_0 + \sin\phi_1}$	$\approx \frac{2.3}{\sin\phi_0} - 0.8 - 3.5\frac{\tan(0.5\phi_1)}{\tan^2\phi_0}$
S_1/x_1	$\approx 1.37 - 0.37\cos\phi_0 + 0.17\tan\phi_1$	$\approx 0.89 + 0.27\tan\phi_0 + 0.15\tan\phi_1$
$x_1/\Delta H_e$	$= \frac{(2\phi_1 + \sin(2\phi_1)) - (2\phi_0 + \sin(2\phi_0))}{2(\sin^2\phi_0 - \sin^2\phi_1)}$	$= \frac{2}{\tan\phi_0 + \tan\phi_1}$
$\overline{a}_{ret}/g = \frac{\Delta H_e}{S_1}$	$= 0.5(\sin\phi_0 + \sin\phi_1)$	$\approx 1.1 - 0.95\cos\phi_0 + 0.37\tan\phi_1$
$\mu = \frac{\Delta H_e}{x_1}$	$\approx 0.02 + 0.9\sin(0.5\phi_0) + 1.05\sin(0.5\phi_1)$	$= 0.5(\tan\phi_0 + \tan\phi_1)$

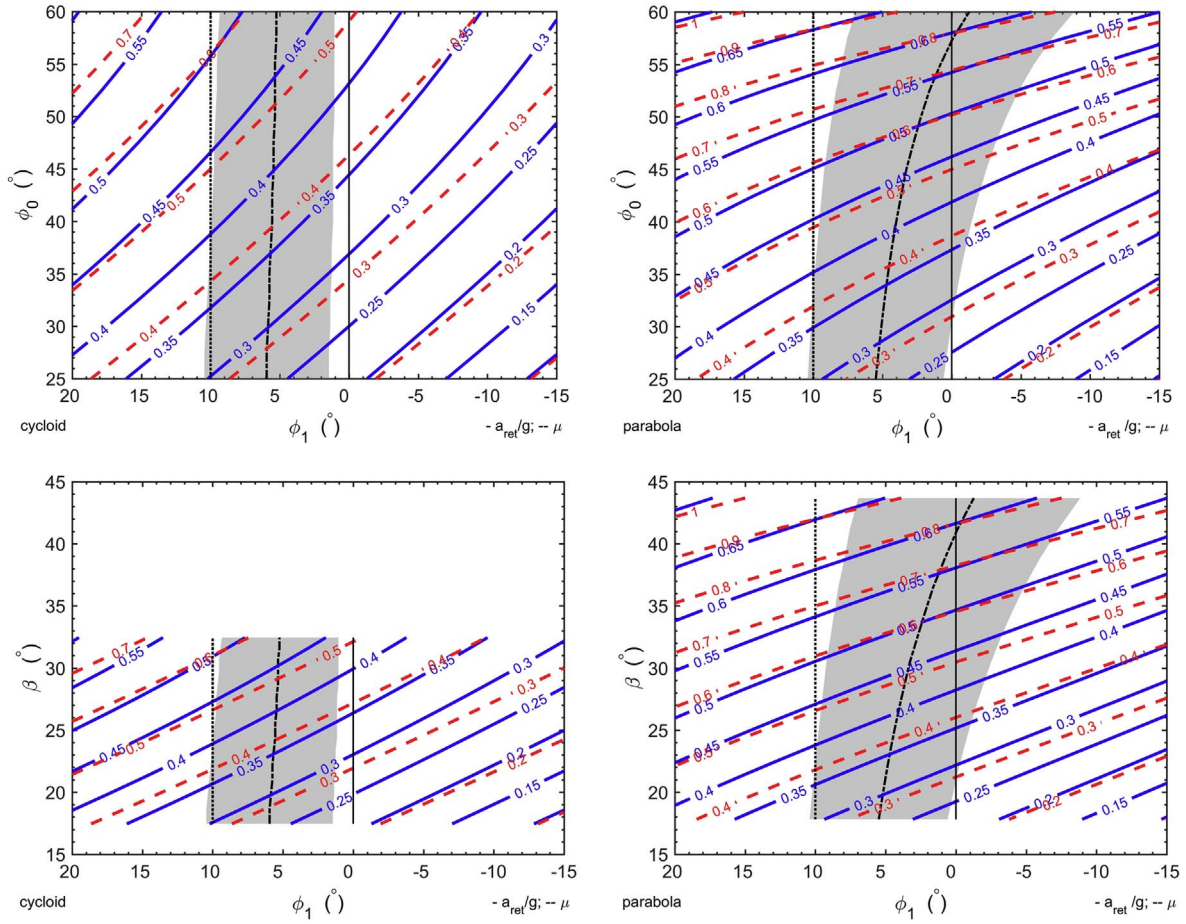

Fig. 11. Contour plots of $\bar{a}_{ret}/g$ (full lines) and μ (dashed lines) depending on ϕ_0 and ϕ_1, which mark the start and stop position. Left panel shows the values for a cycloidal track and right panel for a parabolic one. The black dotted line marks the ϕ_1 angles corresponding to the β-point and dashed-dotted line the one to the α_m-point according to Eq. (1). The gray-shaded area gives the respective ± σ-range. The lower panels show the same as above except with β instead of ϕ_0 as reference.

Table 3
Overview of scaling parameters $U_{\max}$, $\overline{U}$, $\overline{U^2}$, and t_a.

	Cycloid		Parabola	
Parameter	Constant a_{ret}	Coulomb friction	Constant a_{ret}	Coulomb friction
$\frac{U_{\max}}{\sqrt{\frac{gH_{sc}}{2}}}$	$= \left(1 - \frac{\sin\phi_1}{\sin\phi_0}\right)$	$\approx \left(\frac{0.044 + 0.9\phi_0 - 0.92\phi_1}{\sin\phi_0}\right)$	$\approx 1.05 + 0.16\tan\Phi_1 - 0.15\tan\Phi_0 - 1.1\frac{\tan\Phi_1}{\tan\Phi_0}$	$= \left(1 - \frac{\tan\phi_1}{\tan\phi_0}\right)$
$\frac{\overline{U}}{U_{\max}}$	$= 2/\pi$	$\approx 2/\pi$	$\approx 2/\pi$	$\approx 2/\pi$
$\frac{\sqrt{\overline{U^2}}}{U_{\max}}$	≈ 0.81	≈ 0.81	≈ 0.81	≈ 0.81
$\frac{t_a}{\pi\sqrt{2H_{sc}/g}}$	$= 1/\sin\phi_0$	$\approx \frac{(0.77 + 0.22\cos\Phi_0)}{\sin\Phi_0} \times (1 - 0.28\sin\Phi_0\tan\Phi_1)$	$\approx 0.52 + 0.81\ \cot\phi_0 + 0.43\ \tan\phi_1$	$\approx \frac{(0.41 + 0.58\cos\phi_0)}{\sin\phi_0}$

and 0.7 depending on the mean slope angle. Therefore, the order of magnitude for $a_2 H_{sc}$ should be $\lesssim 1$. That means a_2 should scale with H_{sc} and follow $a_2 \propto 1/H_{sc}$. This deliberation is in accordance with the requirement for the maximum velocity of these models that

$$\frac{U_{\max}}{\sqrt{gH_{sc}}} = \sqrt{\frac{1}{a_2 H_{sc}}}\sqrt{\sin\phi_m - \mu\cos\phi_m} \sim \frac{1}{\sqrt{2}}, \tag{103}$$

where $-\tan\phi_m$ is gradient of the track where maximum velocity is reached. Both requirements and the runout observations of avalanches suggests that the velocity dependency might be lower than commonly proposed and that the retardation is either dominated by a rather constant a_{ret} or by Coulomb friction. The latter is in line with suggestions by Ancey and Meunier (2004). Both conditions, Eqs. (102) and (103) are necessary but not sufficient to determine an unique set of parameters $\{\mu, a_2\}$, but they show their interrelation as well as the dependency of the parameters on the steepness of the track. For example, for an avalanche reaching the low point on cycloidal track, numerical simulations suggest that the combination

$$\{\mu; a_2 H_{sc}\} = \{0.22; 1.7\sin\phi_0 - 0.73\} \quad \text{as well as} \tag{104}$$

$$\{\mu; a_2 H_{sc}\} = \{0.62\sin\phi_0 - 0.14; 0.25\} \tag{105}$$

may provide reasonable results. Similarly, the combinations

$$\{\mu; a_2 H_{sc}\} = \{0.22; -3.2\cos\phi_0 + 3\} \quad \text{or} \tag{106}$$

$$\{\mu; a_2 H_{sc}\} = \{0.47\tan\phi_0 - 0.07; 0.25\} \tag{107}$$

give suitable approximations for a parabolic track. As indicated above,

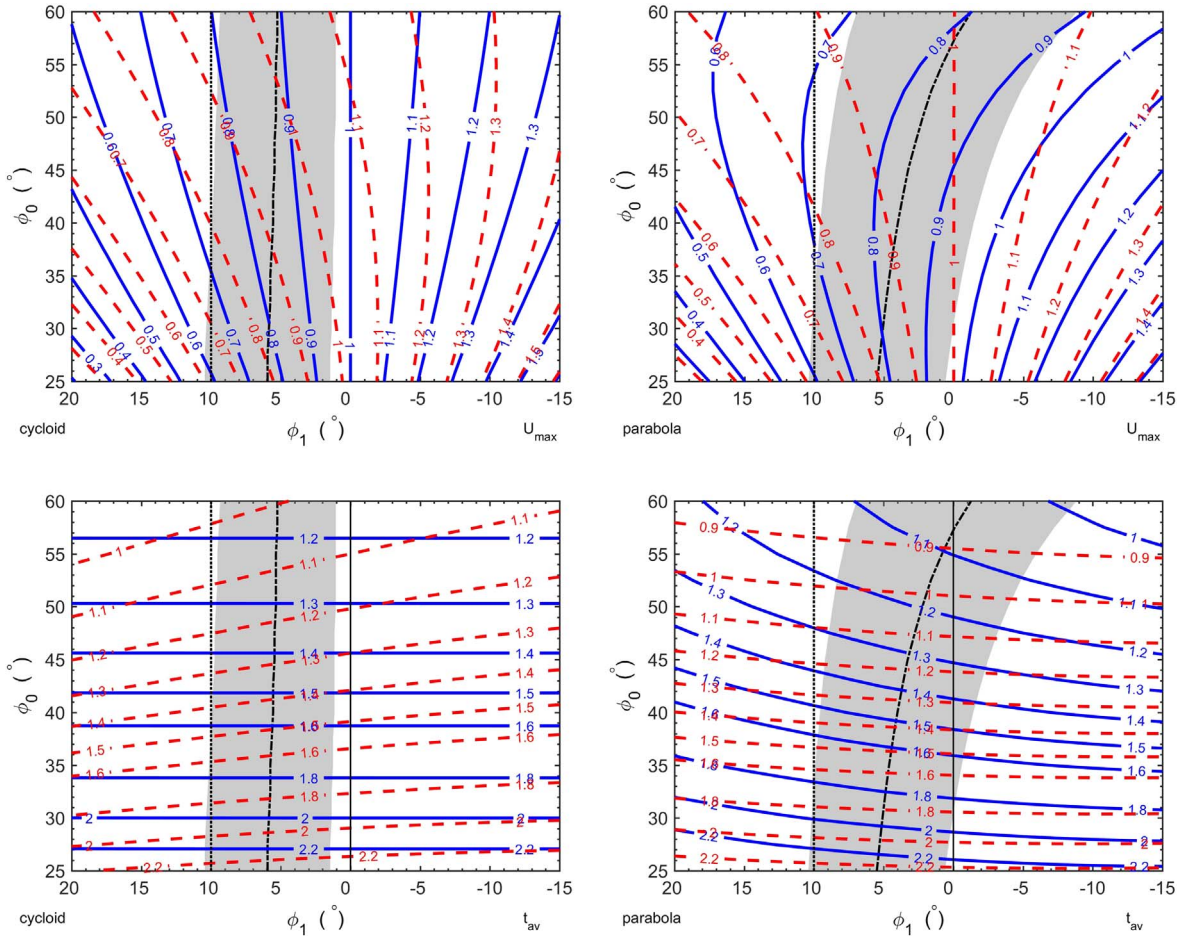

Fig. 12. Top row, contour plots of maximum velocity $U_{\max}/\sqrt{gH_{sc}/2}$ for constant a_{ret} (full lines) and Coulomb friction (dashed lines). Bottom row, comparison of travel time $t_a/(\pi\sqrt{2H_{sc}/g})$ for constant a_{ret} (full line) and Coulomb friction (dashed line). The left panels show the comparison for a cycloidal track and right panels for a parabolic one. The black dotted line marks the ϕ_1 angles corresponding to the β-point and dashed-dotted line the one to the α_m-point according to Eq. (1). The gray-shaded area gives the respective $\pm\,\sigma$-range.

this kind of velocity dependency introduces a scale dependency of the friction parameter a_2. For more discussion on this topic, we refer to (Gauer, 2013, 2014).

Table 3 provides an overview of the obtained scaling relations for $U_{\max}$, $\overline{U}$, $\overline{U^2}$, and t_a with respect to the track type and to the assumed friction model, either constant $\overline{a}_{ret}$ model or Coulomb-friction.

Fig. 12 gives an illustration of the dependency of $U_{\max}$ and t_a on ϕ_0 and ϕ_1 for the two track types. The corresponding friction parameter are shown in Fig. 11. Roughly speaking, both models can provide quite similar results. There are, however, some subtle difference regarding the behavior with respect to the track type. One may say, the Coulomb frictional model on a parabolic track reflects the scaling behavior of a constant a_{ret} model on a cycloid. That is, the Coulomb model on a parabola is almost isochronous like the constant a_{ret} model on a cycloid, and the velocity scalings show similar tendencies. Although, for similar conditions, the Coulomb frictional model tend in many cases to reach slightly higher velocities. This is also reflected in Fig. 13, which shows a contour plot of $U_{\max}$ directly versus α- and β-angle for a parabolic track. This parametrization might be more familiar for practitioners. Again, all runouts with α in the gray area or to the right of it reflect large or "major" events (size R4 or R5). Like the probability decreases to observe runouts to the right of the gray area, decreases the probability to observe corresponding high velocities likewise.

Fig. 14 shows the velocity of a mass block moving with a constant retarding acceleration along a cycloidal track. The retarding acceleration is in the way chosen that the mass block stops at the β-point (which

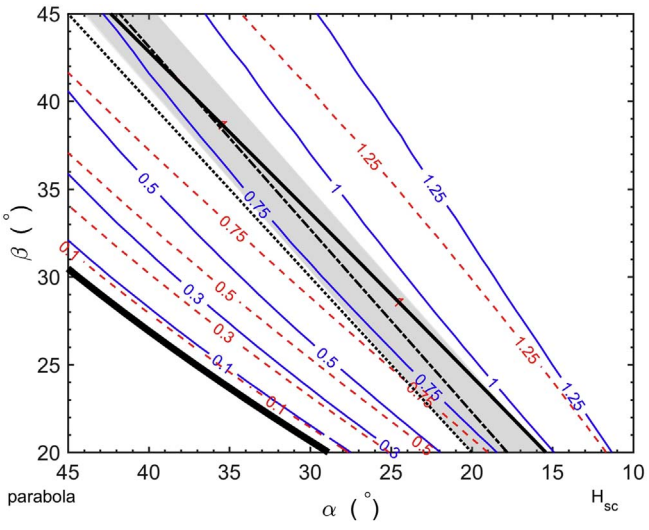

Fig. 13. Contour plots of $U_{\max}/\sqrt{gH_{sc}/2}$ for constant a_{ret} (full lines) and Coulomb friction (dashed lines) depending on the runout angle α. As a reference, the β-points (dotted line), α_m-points (black dashed-dotted line) and the $\pm\,\sigma$ range (gray shaded area) according Eq. (1) are shown (for explanation see Lied and Bakkehøi, 1980). The black line marks the low point (i.e. α_c) and the fat black line marks the "release area".

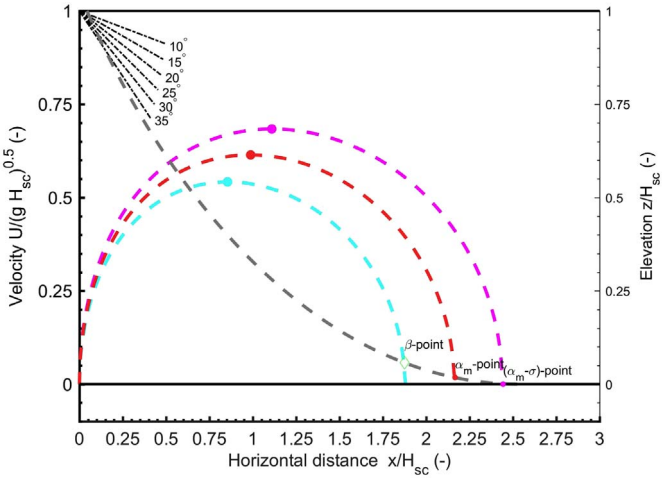

Fig. 14. Velocity of a mass block moving with a constant retarding acceleration along a cycloidal track (gray dashed line; $\phi_0 = 40^\circ$) and reaching 1) the β-point (cyan dashed line), 2) α_m-point (red dashed line), and 3) α_m-σ-point (magenta dashed line). The corresponding maximum velocities are marked with a •. Note, the velocity here is scaled by $\sqrt{gH_{sc}}$. (For interpretation of the references to color in this figure legend, the reader is referred to the web version of this article.)

is close to the $\alpha_m + \sigma$ -point), the α_m-point, or at the $\alpha_m - \sigma$ -point. In these cases, the corresponding maximum velocity $U_{\max}/\sqrt{g\,H_{sc}}$ range between 0.54 and 0.68.

4. Comparison to measurements and observations

In this section, we briefly discuss how the derived scaling behavior relates to real observations and measurements from avalanches, whereby we mainly focus on dry-mixed avalanches as these often combine a relative long runout and high velocity. To make the connection, we qualitatively compare avalanche measurements of runout and front-velocity with results from the scaling analysis. Thereby, we use a more descriptive or exploratory statistics approach; focus of this paper is not a detailed inferential analysis of avalanche data. One remark in advance, avalanche size class R5 considers by definition rare events. This causes that more often than not measurements and direct observations of avalanches are tending to be biased by smaller sizes.

At first, Fig. 15 presents several proposed α-β model relationships for various mountain regions, which involve a wide range of drop heights. In addition both relations, the one for the cycloid and the one for parabola (see Table 2 or Eqs. (23) and (77)) are included. Despite the variety of the data sets and the difference between idealized and real avalanche tracks (e.g. the track in Ryggfonn is neither ideal parabola nor cycloid), the data are in reasonable accordance with the given scaling. As indicated in Fig. 11, where the gray shaded area marks the $\pm\,\sigma$ range of runout observations according to the α-β model (1), the choice of α_c as a reference for the comparison might be a rather conservative but reasonable. According to Fig. 11, α_c, representing the low point of the parabola or cycloid (i.e. $\phi_1 = 0$), might by closer $\alpha_m - \sigma$ than to α_m. This is also reflected in Fig. 15.

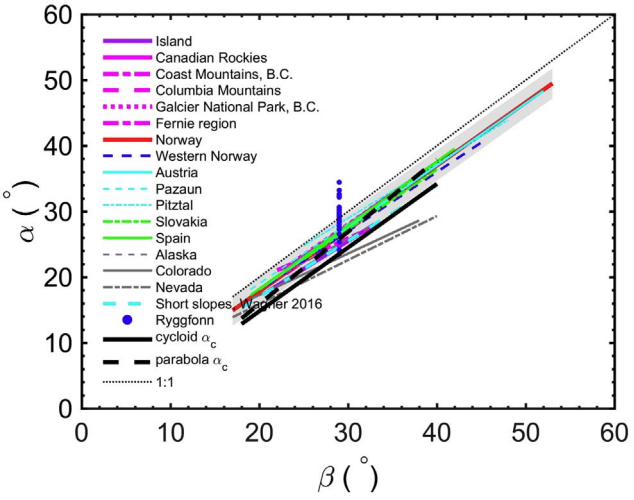

Fig. 15. Comparison of proposed α-β relations for several mountain ranges (data adapted from McClung and Mears, 1991; Wagner, 2016, and references therein). The gray-shaded area marks $\pm\,\sigma$-range corresponding to the Norwegian relation (1). In addition, α values from avalanches at the Ryggfonn test-site are shown.

In the case of avalanches, it is worthwhile to note that due to the strong dependency of the α-angles on the steepness of the respective avalanche path, the sole mentioning of the α-angle as a characteristic for the runout length is actually little informative. Only the connection with a characteristic of the track such as the β-angle provides a sufficient reference to relate α-values to extraordinary events. An exception might be, if α-angles of a specific path/release area are compared to each other. In Fig. 15, this is indicated for avalanches at Ryggfonn with different return periods.

One further remark, Lied and Bakkehøi (1980) argued for choice of the β-point: *"The* 10° *point was chosen because it seems to correspond to the lowest value of the dynamic friction coefficient,μ, in avalanche snow* ($\mu \approx \tan 10^\circ$) *. The exact value ofμis not known and is unimportant here. The main reason for choosing* 10° *is that at slope angles around this value, it seems likely that retardation sets in."* This is still a common misconception, although the simple calculations above suggest and avalanche measurements (Gauer, 2014; Sovilla et al., 2010) show that (almost) all avalanches already start to decelerate on much steeper slopes. On the other hand, most major avalanche events surpass the β-point and they come to rest below this point, as the α-β model implies.

Fig. 16 illustrates the comparison of measured front-velocities from major avalanche events in various tracks with simple mass block calculations. For details on the measurements, we refer to (Gauer, 2012,

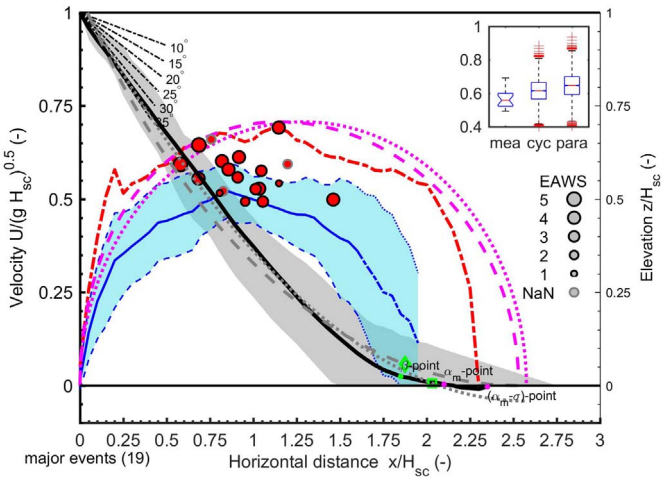

Fig. 16. Range of front-velocities, $U/\sqrt{g\,H_{sc}}$, along the track for a compilation of measurements from various (major) avalanches. Blue line shows the mean, the blue dash lines the $\pm\,\sigma$-range and the red dashed line the maximum observed velocity. The red dots mark the maximum of the different measurements whereby the marker size indicates the EAWS size. The black line represents a "mean path" geometry and the gray shaded area the envelope of all geometries. As a reference, the β-point, α_m and α_m-σ are shown (for explanation see Lied and Bakkehøi, 1980). In addition, the velocity distribution is given for a simple mass block model with constant α_{ret} (dashed magenta line) along a cycloidal track (dashed gray line; $\phi_0 \approx 47^\circ$) and with Coulomb friction (dotted magenta line) along a parabolic track (dotted gray line; $\phi_0 \approx 40^\circ$). The inset shows the variation of the measured maximum front-velocities, $U_{\max}/\sqrt{g\,H_{sc}}$ (mea), and the distribution of the expected maximum velocity for the cycloid (cyc) and the parabola (para) corresponding to $\alpha \sim N(\alpha_m, \sigma^2)$. (For interpretation of the references to color in this figure legend, the reader is referred to the web version of this article.)

2013, 2014). To facilitate a comparison, the path geometries are scaled by the fall height H_{sc} and the velocity as $U/\sqrt{g\ H_{sc}}$. Then the mean of the observed velocities and their standard deviations are calculated at each point along the track. Similarly, an averaged path profile is calculated, which could be regarded as a kind of "standard path". The presented data comprise avalanche tracks with drop heights between 120 m and 1220 m. The EAWS size might be best expressed as

$$\text{EAWS} = \lfloor \log_{10}(V_{Dep}) \rfloor - 1, \tag{108}$$

where V_{Dep} is the volume of the deposit. Thus, an increase of one EAWS size corresponds to an increase in volume of a factor of the order of 10.

For the simulation, the "mean path" was either fitted to a cycloid or to a parabola. The friction parameters were chosen in that way that the mass block stopped at the low point of the track (at α_c), which is actually longer as one would expect from the α-β model. Along the cycloid we present a run with constant retarding acceleration, $a_{ret}/g \approx 0.37$, and along the parabola one with Coulomb friction $\mu \approx 0.42$. As expected from the choice of the friction parameters the maximum velocity is slightly above the measured ones, nonetheless the simulations are in accordance with the measurements. As example, for the cycloidal fit, $\phi_0 \approx 47^\circ$ and the expected $\phi_1 \approx 5.3^\circ$ corresponding to the mean α-angle according to Eq. (1). Now, using Eq. (36) provides $U_{\max}/\sqrt{gH_{sc}} \approx 0.62$, which is in agreement with the measurements. The inset shows an extended comparison between the measured maximum front-velocities and the expected maximum velocities according to the variation σ of the expected α_m-angles. The comparison is done for a cycloid and a constant a_{ret} model as well as for a parabola and a Coulomb model by using a Monte-Carlo approach and assuming a normal distribution $\alpha \sim N(\alpha_m, \sigma^2)$. By keeping in mind that the measurements are probably biased to smaller relative sizes and their tracks are not idealized, the accordance between measurements and models is surprisingly good.

Also the comparison of the range of measurements in Fig. 16 with our example in Fig. 14, which shows calculations for the same cycloid, supports that the scaling is consistent with our measurements.

Finally, Fig. 17 depicts an extended collection of observed maximum front-velocities of dry-snow/dry-mixed avalanches from various sites around the globe. Data originate, among others, from Ryggfonn

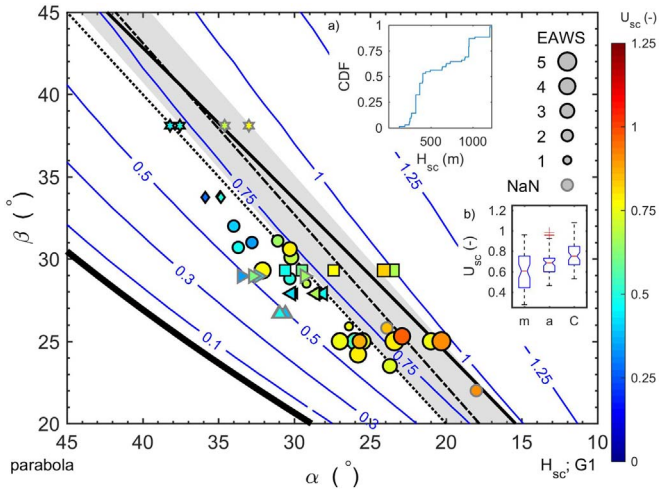

Fig. 17. Scaled maximum front-velocities $U_{\max}/\sqrt{gH_{sc}/2}$ (color coded) of dry-mixed avalanches: compilation of measurements from various sites around the globe. As reference, the β-points (dotted line), α_m-points (black dashed line) and the $\pm\,\sigma$ range (gray shaded area) according Eq. (1) are shown (for explanation see Lied and Bakkehøi, 1980). The blue lines show the expected maximum front-velocities with a_{ret} = const. on a parabolic track. The fat black line marks the "release area". Marker size indicates the avalanche size following the EAWS size classification. Inset a) shows the cumulative distribution of H_{sc} to give an impression of the underlying data. Inset b) shows the variation of the measured (m) maximum front-velocities, $U_{\max}/\sqrt{g\ H_{sc}/2}$, and the corresponding distribution of the maximum velocity for a model with constant a_{ret} (a) and a Coulomb model (C) on a parabola.

(□), Vallée de la Sionne, Lukamanier, Col de Lautaret (△,▷), Rogers Pass (★), and Takahira (◇). References to the data can be found in, e.g., (Gauer, 2012, 2013, 2014, and references therein) as well as in (Shoda, 1966; Gubler et al., 1986; Schaerer, 1973; McClung and Schaerer, 1983; Schaerer and Salway, 1980; Eybert-Berard et al., 1978; LaChapelle and Lang, 1980; Nettuno, 2004). Sites from where a series of measurements are available are marked separately. The measurements were done with various methods such as timing between know points, filming, or RADAR measurements. In contrast to the data in Fig. 16, not in all cases, the front-velocity was followed along the whole profile, which can cause a slight underestimation of the real maximum value. Also, not all of these avalanches are major events relative to the path (i.e. size R4 or R5); or roughly spoken, not all of those avalanches surpassed the β-point.

Despite the variety of measurement methods and the variety of tracks, most of which are not perfect parabolas, and despite the variation of ambient conditions and sizes (drop height as well as volume), the data are in general accordance with the proposed scaling behavior, especially with the model with a_{ret} = const. For a pure Coulomb model, one would by trend expect slightly higher velocities (see Fig. 13). This can also be seen in the inset b). It shows the variation of the measured maximum front-velocities, $U_{\max}/\sqrt{g\ H_{sc}/2}$ (m), and the distribution of the corresponding maximum velocities for a model with constant a_{ret} (a) and a Coulomb model (C) on a parabola with α and β values corresponding to the measurements. As in Fig. 16, here too, the measurements tend to be slightly below the model values for the idealized tracks.

5. Conclusions

In this paper, we studied the scaling behavior of a simple avalanche model along idealized tracks and compared the results with a wide range of avalanche observations and measurements regarding runout distance and maximum front-velocity. For major events, we found $U_{\max} \sim \sqrt{g\ H_{sc}/2}$. The corresponding travel time of the avalanche front $t_{av} \sim 2\sqrt{H_{sc}}$ (in s), however, it is depending of the mean slope angle. On a shallower track avalanches take longer. Admittedly, our mass block model and the idealization of real avalanche tracks as smooth 2-dimensional cycloids or parabolas is a huge oversimplification; no avalanche path is perfect a cycloid nor parabola, which makes a one-to-one comparison difficult. Nonetheless, this first order approximation reproduces a series of observations and measurements on dry-mixed avalanches surprisingly well. Therefore, the scaling can provide practitioners with a useful first guess on the expected velocity of dry-mixed avalanches. Wet-snow avalanches will probably behave differently as measurements suggest (e.g. Gauer and Kristensen, 2016; Steinkogler et al., 2014). The consistency between model and observations/measurements suggests, firstly, a strong dependency of the apparent retardation on the mean steepness of the track, for which the β-angle might be a proxy. Secondly, the contributions of snow erosion (Gauer and Issler, 2004; Sovilla et al., 2006), snowpack properties (Steinkogler et al., 2014), or the avalanche size (Gauer et al., 2010; Gauer, 2016) to the retardation seem to be of second order. That does not mean these effects are not important; they are determining the return period of the actual runout distance in a specific avalanche path. Therefore, the particular snowpack properties and the relative avalanche size may matter.

Our results are in line with those of Ancey (2005), although, he focused his analysis on only seven avalanche tracks with total fall heights between 1000 m and 1900 m and a mean $\beta \approx 25^\circ$ ($\sigma = 4.3^\circ$). He also did not include velocity measurements in his analysis.

Our scaling analysis does not provide direct insight of the rheology of (dry-mixed) avalanches. Nonetheless, it can provide constraints to it; that is, combined observations on, S_1, $U_{\max}$, and t_a will give indication on the flow behavior. In any case, the velocity scaling and the

dependency of the retardation on the mean slope angle needs to be reflected in avalanche models.

The indicated scaling behavior also implies that conclusions drawn from avalanche measurements originating from a limited number of paths (test-sites) need to be interpreted with care as long as no further cross-comparisons between different avalanche paths (test-sites) have been undertaken, which could uncover possible underlying scaling relations. But also results from small-scale granular and snow-slide tests need to be interpreted taking into account avalanche measurements, observations, and the presented scaling.

Acknowledgments

Parts of this research was financially supported by the Norwegian Ministry of Oil and Energy through the project grant “R&D Snow avalanches 2017–2019” to NGI, which is administrated by the Norwegian Water Resources and Energy Directorate (NVE). The author thanks Peter Schaerer for providing some of the Rogers Pass data. The comments of two anonymous reviewers have been highly appreciated and taken into account.

References

Ancey, C., 2005. Monte Carlo calibration of avalanches described as Coulomb fluid flows. Philos. Trans. R. Soc. A Math. Phys. Eng. Sci. 363, 1529–1550.

Ancey, C., Meunier, M., 2004. Estimating bulk rheological properties of flowing snow avalanches from field data. J. Geophys. Res. Earth Surf. 109, 1–15 F01004.

Bakkehøi, S., Domaas, U., Lied, K., 1983. Calculation of snow avalanche runout distance. Ann. Glaciol. 4, 24–29. http://dx.doi.org/10.1017/S0260305500005188.

Christen, M., Kowalski, J., Bartelt, P., 2010. RAMMS: numerical simulation of dense snow avalanches in three-dimensional terrain. Cold Reg. Sci. Technol. 63, 1–14.

Coaz, J.W.F., 1910. Statistik und Verbau der Lawinen in den Schweizeralpen. Stämpfli & Cie, Bern etc. With plates and maps.

Eybert-Berard, A., Perroud, P., Brugnot, A., Mura, R., Rey, L., 1978. Mesures dynamiques dans l’avalanche résultats expérimentaux du col du lautaret (1972–1978). In: ANENA (Ed.), Proceedings of the Second International Meeting on Snow and Avalanches, 12–14 April 1978, Grenoble, France. 2nde Rencontre Internationale sur la Neige et les Avalanches Societé Hydrotechnique de France, Grenoble. ANENA, Grenoble, France, pp. 203–224.

Gauer, P., 2012. On avalanche (front) velocity measurements at the Ryggfonn avalanche test site and comparison with observations from other locations. In: Proceedings of the International Snow Science Workshop, 2012, September 16-21, 2012 at the Denali Center in Anchorage, Alaska, pp. 427–432.

Gauer, P., 2013. Comparison of avalanche front velocity measurements: supplementary energy considerations. Cold Reg. Sci. Technol. 96, 17–22.

Gauer, P., 2014. Comparison of avalanche front velocity measurements and implications for avalanche models. Cold Reg. Sci. Technol. 97, 132–150.

Gauer, P., 2016. Selected observations from avalanche measurements at the Ryggfonn test site and comparisons with observations from other locations. In: Proceedings of the International Snow Science Workshop 2016, Breckenrigde, CO, pp. 1340–1347.

Gauer, P., Issler, D., 2004. Possible erosion mechanisms in snow avalanches. Ann. Glaciol. 38, 384–392.

Gauer, P., Issler, D., Lied, K., Kristensen, K., Sandersen, F., 2008. On snow avalanche flow regimes: inferences from observations and measurements. In: Proceedings of the International Snow Science Workshop 2008, September 21- 27, Whistler, British Columbia, Canada, pp. 717–723.

Gauer, P., Kristensen, K., 2016. Four decades of observations from NGI's full-scale avalanche test site Ryggfonn – summary of experimental results. Cold Reg. Sci. Technol. 125, 162–176.

Gauer, P., Kronholm, K., Lied, K., Kristensen, K., Bakkehøi, S., 2010. Can we learn more from the data underlying the statistical α-β model with respect to the dynamical behavior of avalanches? Cold Reg. Sci. Technol. 62, 42–54.

Greene, E., Atkins, D., Birkeland, K., Elder, K., Landry, C., Lazar, B., McCammon, I., Moore, M., Sharaf, D., Sternenz, C., Tremper, B., Williams, K., 2016. Snow, weather, and avalanches: observation guidelines for avalanche programs in the United States. In: Tech. rep. American Avalanche Association.

Gubler, H., Hiller, M., Klausegger, G., Suter, U., 1986. Messungen an Fliesslawinen. Zwischenbericht. In: Internal report 41. Swiss Federal Institute for Snow and Avalanche Research.

Heim, A., 1932. Bergsturz und Menschenleben. In: Geologische Nachlese Nr. 30. Beiblatt zur Vierteljahrsschrift der Naturforschenden Gesellschaft in Zürich 77. Naturforschenden Gesellschaft, Zürich, pp. 220.

LaChapelle, E.R., Lang, T.E., 1980. A comparison of observed and calculated avalanches. J. Glaciol. 25 (92), 309–314.

Lied, K., Bakkehøi, S., 1980. Empirical calculations of snow-avalanche run-out distance based on topographic parameters. J. Glaciol. 26 (94), 165–177.

McClung, D., Schaerer, P., 2006. The Avalanche Handbook, 3rd edition. The Mountaineers Books, 1011 SW Klickitat Way, Seattle, Washington 98134.

McClung, D.M., Mears, A.I., 1991. Extreme value prediction of snow avalanche runout. Cold Reg. Sci. Technol. 19 (2), 163–175 May.

McClung, D.M., Schaerer, P., 1983. Determination of avalanche dynamics friction coefficients from measured speeds. Ann. Glaciol. 4 (1), 170–173.

Moner, I., Orgue, S., Gavalda, J., Bacardit, M., 2013. How big is big: results of the avalanche size classification survey. In: Proceedings of the International Snow Science Workshop Grenoble–Chamonix Mont-Blanc - 2013.

Nettuno, L., 2004. Field measurements and model calibration in avalanche dynamics. Surv. Geophys. 16 (5-6), 635–648.

Perla, R., Cheng, T.T., McClung, D.M., 1980. A two-parameter model of snow-avalanche motion. J. Glaciol. 26 (94), 119–207.

Sampl, P., Granig, M., 2009. Avalanche simulation with SAMOS-AT. In: Proceedings of the International Snow Science Workshop, Davos, pp. 519–523.

Schaerer, P.A., 1973. Observations of avalanche impact pressures. In: Perla, R. (Ed.), Advances in North American Avalanche Technology. Vol. RM-GTR-3:. US Dept. Agriculture, Forest Service, Rocky Mountain Forest and Range Experiment Station, 1973, pp. 51–54 in: Proceedings of Usda Forest Service National Avalanche Training Program, Reno, Nev, November 16-17, 1972: Forest Service General Technical Report Rm-3, P 51-54, September 1973. 2 Fig. 1 Tab, 3 Ref.

Schaerer, P.A., Salway, A.A., 1980. Seismic and impact-pressure monitoring of flowing avalanches. J. Glaciol. 26 (94), 179–187.

Shoda, M., 1966. An experimental study on dynamics of avalanches snow. In: Tison, L.J. (Ed.), International Symposium on Scientific Aspects of Snow and Ice Avalanches. Vol. 69 of IAHS Publ. Int. Assoc. Hydrol. Sci., Gentbrugge, Belgin, pp. 214–229.

Sovilla, B., Burlando, P., Bartelt, P., 2006. Field experiments and numerical modeling of mass entrainment in snow avalanches. J. Geophys. Res. Earth Surf. 111, 1–16 F03007.

Sovilla, B., McElwaine, J.N., Schaer, M., Vallet, J., 2010. Variation of deposition depth with slope angle in snow avalanches: measurements from Vallée de la Sionne. J. Geophys. Res. Earth Surf. 115, 1–13 F02016.

Steinkogler, W., Sovilla, B., Lehning, M., 2014. Influence of snow cover properties on avalanche dynamics. Cold Reg. Sci. Technol. 97, 121–131.

Voellmy, A., 1955. Über die Zerstörungskraft von Lawinen. Schweizerische Bauzeitung Sonderdruck aus dem 73. Jahrgang (12, 15, 17, 19 und 37). pp. 1–25.

Wagner, P., 2016. Kalibrierung des α-β-Modells für das Ermitteln der Auslauflänge von kleinen und mittleren Lawinen. Institut für Alpine Naturgefahren (IAN), BOKU-Universität für Bodenkultur Master thesis.